A process study of tidal mixing over rough topography

Young Ro Yi*, Sonya Legg† and Robert Nazarian†

*Geosciences Department,
†Atmospheric and Oceanice Sciences Program,
Princeton University
yryi@princeton.edu

Abstract

Tidal flow over topography generates internal waves at the tidal frequency called internal tides, and the breaking of these waves enhances the dissipation of energy and diapycnal mixing over rough topography. Tidal mixing must be parameterized in climate models since mixing processes occur on subgrid spatial scales. However, these parameterizations lack spatial variations in the fraction of the tidal energy which is locally dissipated (q) and the vertical distribution of the dissipation ($F(z)$). We present results from 2-D numerical simulations demonstrating the sensitivity of q and $F(z)$ to the Coriolis frequency, topographic wavelength and relative steepness, and highlight the need to include these parameters in tidal mixing parameterizations used in large-scale ocean models.

1 Introduction

The generation and breaking of internal tides lead to enhanced energy dissipation and diapyncal mixing over rough topography (Polzin et al., 1997). This mixing sustains and influences the global ocean circulation and can affect the large-scale climate through changes to the ocean heat and salt distribution, carbon uptake and sea level (Munk and Wunsch, 1998; Hallberg et al., 2013).

Current general circulation models (GCMs) often use a simple dissipation parameterization introduced in St. Laurent et al. (2002) along with the diffusivity formulation from Osborn (1980):

$$\epsilon = \frac{qE(x,y)F(z)}{\rho} \tag{1}$$

$$\kappa = \frac{\Gamma\epsilon}{N^2} \tag{2}$$

where ϵ is the rate of turbulent energy dissipation, $E(x,y)$ is the energy transfer rate from barotropic to baroclinic tides, q is the fraction of energy input used locally for dissipation, $F(z)$ is a structure function describing the vertical distribution of this dissipation, ρ is a reference density, κ is the turbulent diffusivity, Γ is a mixing efficiency often set to 0.2, and N^2 is the stratification. However, (1) fails to account for two major details about ϵ: ***(i)*** spatial and temporal variations in q and ***(ii)*** lateral variations in $F(z)$.

Currently q is fixed at 30% globally, and $F(z)$ is assumed to be an exponential decay from the ocean floor with a 500 m decay scale based on observations from the Brazil Basin (St. Laurent et al., 2001). A numerical study by Melet et al. (2013) demonstrated that the ocean circulation is sensitive to changes to the vertical distribution of ϵ. Observations and numerical studies have both noted that nonlinear wave-wave interactions (including parametric subharmonic instabilities; henceforth PSI) transfer energy to smaller spatial

scales, leading to enhanced levels of dissipation (MacKinnon and Winters, 2005; MacKinnon et al., 2013a,b; Nikurashin and Legg, 2011). These interactions can make $F(z)$ deviate significantly from an exponentially decaying curve. In this paper, we present the results of a parameter space study of tidal mixing over rough topography, with a focus on the effects of parameters such as the Coriolis frequency (f_0), topographic wavelength (λ_k) and relative steepness (γ) on q and $F(z)$.

2 Model description

Two-dimensional numerical simulations were performed using the nonhydrostatic MIT general circulation model (MITgcm) (Marshall et al., 1997). The model domain was 60 km wide and 4 km deep with horizontal and vertical resolutions of 30 m and 10 m respectively. The bottom topography was sinusoidal, and a body-force was applied at the lunar semidiurnal (M2) tidal frequency. Horizontal periodic boundaries were employed to simulate an infinitely wide ocean. A linear equation of state depending only on temperature was used, and a constant stratification was assumed. A sponge layer in the top one kilometer of the domain prevented reflection of internal waves, focusing on dissipation due to the internal waves that were generated and broke near the bottom. Four values of f_0 ranging from 0 to 10^{-4} s^{-1}, spanning the equator to regions poleward of the critical latitude of 28.7°, four values of γ including subcritical, critical and supercritical topographies, and six different values of λ_k ranging from 2.5 km to 15 km were used for a total of ninety-six unique experiments.

The turbulent energy dissipation was calculated from MITgcm output as:

$$\epsilon = \nu_i \left\langle \left(\frac{\partial u_j'}{\partial x_i} \right)^2 \right\rangle \tag{3}$$

where ν_i represents the kinematic viscosities in each direction and u_j' the perturbation velocities due to the waves. The angular brackets represent an average over tidal cycles. The tidal energy conversion rate was calculated as:

$$E(x,y) = \int_{x=0}^{x=L_x} p'(x, z{=}h(x), t) U_{bt}(x,t) \frac{dh}{dx} dx \tag{4}$$

where L_x is the domain width, $p'(x, z{=}h(x), t)$ is the pressure perturbation along the top of the topography due to the waves and $U_{bt}(x,t)$ is the barotropic velocity (Khatiwala, 2003; Legg and Huijts, 2006). The fraction of energy used for dissipation over a certain depth range was calculated as:

$$q = \frac{\rho \int_{z_1}^{z_2} \epsilon dz}{E(x,y)} \tag{5}$$

where z_1 and z_2 are two depths which vary based on the processes of interest (i.e. turbulent boundary layer and PSI).

3 Vertical profiles of energy dissipation

In figures 1 and 2, we observe that $F(z)$ either has $\boldsymbol{(i)}$ regions of enhanced dissipation extending from the bottom or $\boldsymbol{(ii)}$ dissipation that decays steeply away from the bottom. $F(z)$ of the first kind are observed for almost all simulations when $f_0{=}7{\times}10^{-5}$ s^{-1} where PSI is resonant ($f_0{=}\omega/2$). $F(z)$ of the second kind are observed for most of the remaining simulations where PSI is much weaker or nonexistent.

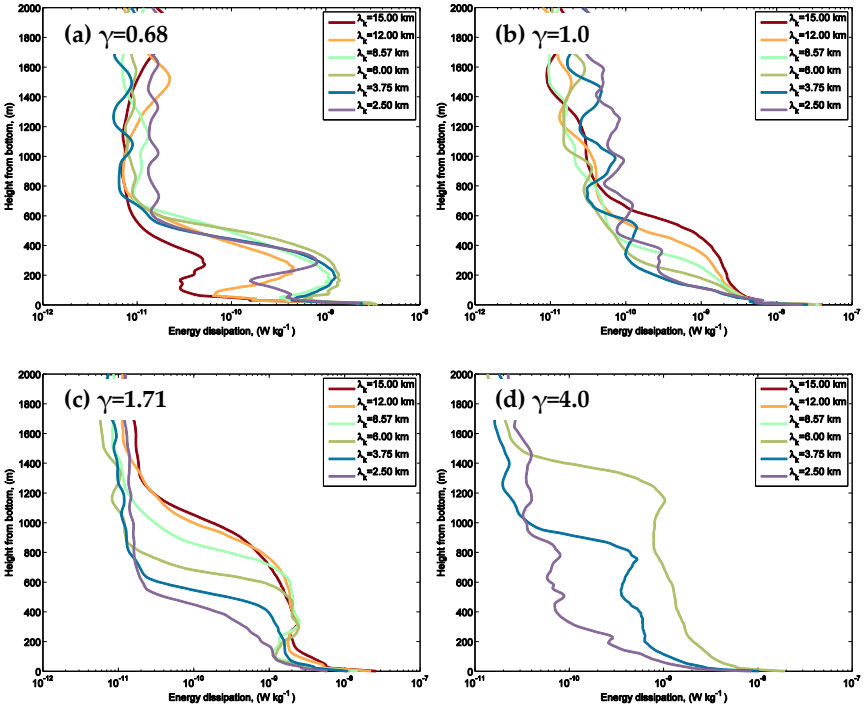

Figure 1: Vertical profiles of energy dissipation (W/kg) from simulations with f_0=7×10^{-5} s^{-1} but with different values of λ_k. The values of γ were (a) 0.68, (b) 1.0, (c) 1.71 and (d) 4.0. The y-axis shows height above the bottom (m).

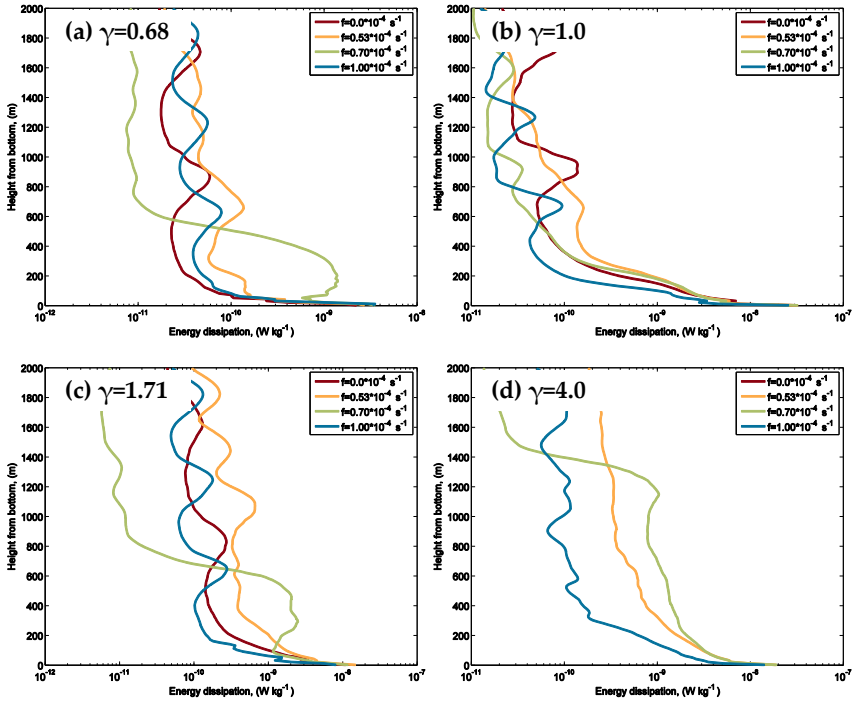

Figure 2: Vertical profiles of energy dissipation (W/kg) from simulations with λ_k=6 km but with different values of f_0. The values of γ were (a) 0.68, (b) 1.0, (c) 1.71 and (d) 4.0. The y-axis shows height above the bottom (m).

4 Local fraction of energy dissipation

In figure 3, we observe that q $(\boldsymbol{i})$ scales inversely with λ_k and $(\boldsymbol{ii})$ peaks at the critical latitude (f_0=7×10^{-5} s^{-1}). The first relationship can be explained by the fact that as λ_k decreases, internal waves of smaller spatial scales are generated. These waves are more prone to instabilities, leading to turbulent dissipation and mixing (see St. Laurent and Garrett (2002) and Garrett and Kunze (2007)). The second relationship due to PSI has been described in previous modeling studies (Nikurashin and Legg, 2011). Additionally, we note that these relationships are modulated by variations to γ. The peak in q at the critical latitude is most evident at subcritical and critical slope topography, while supercritical topography shows less dependence of q on latitude. Balmforth and Peacock (2009) explored how γ affects the tidal energy conversion (4) and stressed how different wave interference patterns can form for supercritical regimes, complicating attempts to parameterize $E(x, y)$ and ϵ.

5 Conclusion

Through a parameter space study using numerical simulations, we have explored the effects of the Coriolis frequency and the bottom topography on the fraction and vertical distribution of tidal energy dissipation used for mixing. Two general groups of $F(z)$ were found: $(\boldsymbol{i})$ those where enhanced dissipation extends from the bottom and $(\boldsymbol{ii})$ those where dissipation decays steeply away from the bottom. This grouping was mostly determined by the presence or absence of resonant PSI. q was found to $(\boldsymbol{i})$ scale inversely with λ_k and $(\boldsymbol{ii})$ peak at the critical latitude with f_0=7×10^{-5} s^{-1}, with changes to γ modifying the strength of these trends. With these relationships in mind, we hope to work towards a most robust tidal mixing parameterization that incorporates spatial variations due to variations of the Coriolis frequency and the seafloor geometry.

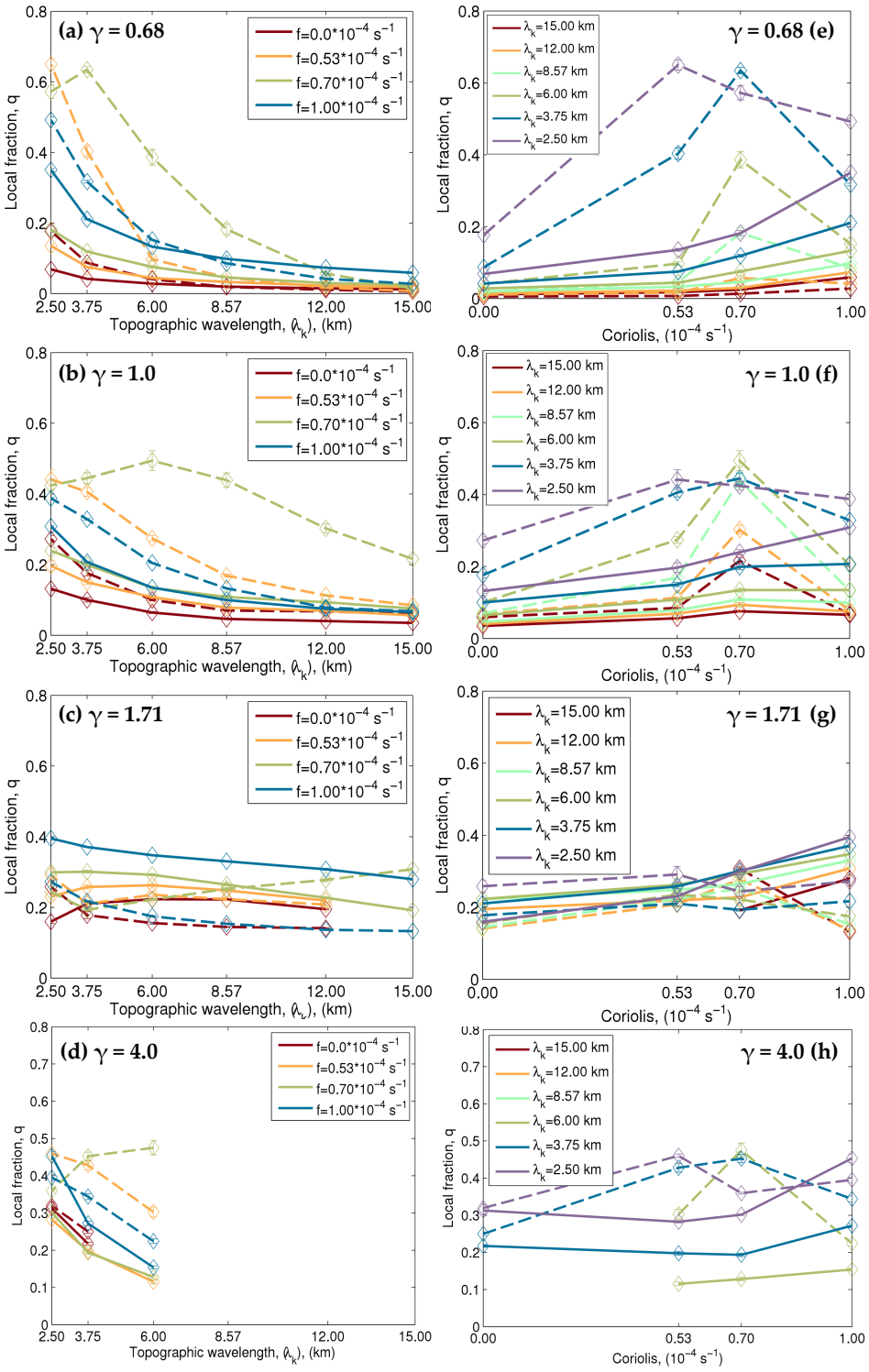

Figure 3: Local fraction of energy dissipation (q) and its errors ($2\times\sigma_{mean}$) plotted versus (a∼d) λ_k (km) and (e∼h) f_0 (10^{-4} s^{-1}). q from 0∼50 m (solid lines) represents the local fraction within the turbulent boundary layer (TBL) near the topography, and q from 50∼2000 m (dashed lines) represents the local fraction above the TBL. Only the experiments with topographic peaks $\leq$ 1000 m were considered.

References

Balmforth, N. J. and Peacock, T. (2009). Tidal conversion by supercritical topography. *J. Phys. Oceanogr.*, 39(8):1965–1974.

Garrett, C. and Kunze, E. (2007). Internal tide generation in the deep ocean. *Annual Review of Fluid Mechanics*, 39(1):57–87.

Hallberg, R., Adcroft, A., Dunne, J. P., Krasting, J. P., and Stouffer, R. J. (2013). Sensitivity of twenty-first-century global-mean steric sea level rise to ocean model formulation. *J. Climate*, 26(9):2947–2956.

Khatiwala, S. (2003). Generation of internal tides in an ocean of finite depth: analytical and numerical calculations. *Deep Sea Research Part I: Oceanographic Research Papers*, 50(1):3–21.

Legg, S. and Huijts, K. M. H. (2006). Preliminary simulations of internal waves and mixing generated by finite amplitude tidal flow over isolated topography. *Deep Sea Research Part II: Topical Studies in Oceanography*, 53(12):140–156.

MacKinnon, J. A., Alford, M. H., Pinkel, R., Klymak, J., and Zhao, Z. (2013a). The latitudinal dependence of shear and mixing in the Pacific transiting the critical latitude for PSI. *J. Phys. Oceanogr.*, 43(1):3–16.

MacKinnon, J. A., Alford, M. H., Sun, O., Pinkel, R., Zhao, Z., and Klymak, J. (2013b). Parametric subharmonic instability of the internal tide at 29N. *J. Phys. Oceanogr.*, 43(1):17–28.

MacKinnon, J. A. and Winters, K. B. (2005). Subtropical catastrophe: significant loss of low-mode tidal energy at 28.9. *Geophys. Res. Lett.*, 32(15):L15605.

Marshall, J., Adcroft, A., Hill, C., Perelman, L., and Heisey, C. (1997). A finite-volume, incompressible Navier Stokes model for studies of the ocean on parallel computers. *J. Geophys. Res.*, 102(C3):5753–5766.

Melet, A., Hallberg, R., Legg, S., and Polzin, K. (2013). Sensitivity of the ocean state to the vertical distribution of internal-tide-driven mixing. *J. Phys. Oceanogr.*, 43(3):602–615.

Munk, W. and Wunsch, C. (1998). Abyssal recipes II: energetics of tidal and wind mixing. *Deep Sea Research Part I: Oceanographic Research Papers*, 45(12):1977–2010.

Nikurashin, M. and Legg, S. (2011). A mechanism for local dissipation of internal tides generated at rough topography. *J. Phys. Oceanogr.*, 41(2):378–395.

Osborn, T. R. (1980). Estimates of the local rate of vertical diffusion from dissipation measurements. *J. Phys. Oceanogr.*, 10(1):83–89.

Polzin, K. L., Toole, J. M., Ledwell, J. R., and Schmitt, R. W. (1997). Spatial variability of turbulent mixing in the abyssal ocean. *Science*, 276(5309):93–96.

St. Laurent, L. C. and Garrett, C. (2002). The role of internal tides in mixing the deep ocean. *J. Phys. Oceanogr.*, 32(10):2882–2899.

St. Laurent, L. C., Simmons, H. L., and Jayne, S. R. (2002). Estimating tidally driven mixing in the deep ocean. *Geophys. Res. Lett.*, 29(23):2106.

St. Laurent, L. C., Toole, J. M., and Schmitt, R. W. (2001). Buoyancy forcing by turbulence above rough topography in the abyssal Brazil Basin. *J. Phys. Oceanogr.*, 31(12):3476–3495.